Journal of Marine Research, 44, 445–471, 1986

On the role of topography in the ocean circulation

by Paola Cessi[1] and Joseph Pedlosky[2]

ABSTRACT

The ideas developed by Rhines and Young (1982a,b) are used to analyze the effect of topography in simple baroclinic models. The presence of longitude-dependent topography induces strong internal jets with transports of the same magnitude as the interior flow. It is shown that the existence of these features is independent of the forcing structure at the top of the model ocean, of the topography form and of the forcing in subsurface layers as long as the latter is small. Some examples are given both for forcings which, in the absence of topography, would give circulations closed in the interior and for forcings that require a western boundary current.

Topography also shifts the line of zero transport allowing for significant flow across the line of zero wind stress curl. Moreover, the lines dividing the subtropical gyre from the subpolar gyre are different in every layer, a feature absent in the flat bottom case.

1. Introduction

In recent years a number of theories of the ocean general circulation have been developed using conservative (quasi) geostrophic dynamics in the interior region of the domain under consideration. Young and Rhines (1982) (YR) and Rhines and Young (1982a) (RYa), using a quasi-geostrophic, large-scale layer model, have shown how the circulation forced by a prescribed Ekman pumping can extend downward through small vertical transfer of horizontal momentum by eddies. Luyten *et al.* (1983) (LPS) proposed a rather different mechanism, in which the subsurface waters are set in motion by ventilation, through outcrop of density surfaces.

All of these models are constrained by the Sverdrup relation between the vertically integrated meridional transport and the wind stress curl. This relation, though, is valid only over a flat bottom, or where the bottom velocity is negligible, and Luyten *et al.* (1985) have shown that in the North Atlantic subpolar gyre, topography has a strong influence on the meridional transport.

The purpose of this study is to analyze the effect of topography on the wind-driven circulation. We will borrow directly the ideas and terminology introduced in YR and RYa.

1. MIT-WHOI Joint Program in Physical Oceanography, Center for Meteorology and Physical Oceanography, Massachusetts Institute of Technology, Cambridge, Massachusetts, 02139, U.S.A.
2. Woods Hole Oceanographic Institution, Woods Hole, Massachusetts, 02543, U.S.A.

We find that large-scale topography, when containing a longitudinal variation, can have a dramatic effect on the deduced circulation patterns in models of wind-driven, stratified ocean flows. First, we show that even the presence of a uniform slope in the x (longitudinal) direction alters the qualitative structure of the Sverdrup problem. Closed geostrophic contours in the lower layer now contain flows which can be matched to the Sverdrup external field only with the intervention of internal boundary currents. We show that this arises whether or not the flow within the girdling geostrophic contour has uniform potential vorticity and thus our results do not depend sensitively on the homogenization arguments of RYa.

We then demonstrate that ridge-like topography, which we think of as a model of mid-ocean ridge topography, will also produce boundary currents embedded in the Sverdrup interior. This phenomenon is fundamentally different from the first case as it depends on strong variations in east-west bottom slope and, in distinction with the previous case, is present in homogeneous models as well.

During the preparation of this manuscript, the work of de Szoeke (1985) came to our attention. De Szoeke has considered the role of uniform east-west slope (our first topic). Although there are many elements in common in the two treatments, the directions taken are quite distinct. We have chosen to emphasize the need to embed the circulation in the dynamics appropriate to an oceanic basin. Therefore, in distinction to de Szoeke we do not accept any deep flow on isolines of potential vorticity which intersect the eastern boundary. Nor do we artificially adjust the wind field to produce closure. This has important consequences for the predicted patterns. Our proposed deep flows *vanish* completely outside the outermost geostrophic contour. We also show that the general character of the flow is independent of homogenization of potential vorticity and thus we do not restrict attention to harmonic topography as does de Szoeke. We wish to emphasize that internal jets form with transport of order 1 both in the interior and at the boundary of the region where the subsurface waters move and such a region is well inside the interior of the basin.

Part of the motivation for considering topography was to examine whether the effects of topography allow geostrophic flow across the line of zero Ekman pumping. We show that this indeed occurs, especially in the case of forcing of realistic amplitude. Moreover, the lines of zero transport are different in each layer, unlike the flat bottom models.

In section 2 we briefly recapitulate the formulation and solution of the quasi-geostrophic two-layer model for the case of constant bottom slope. That is, analogously to YR and RYa we will force the upper layer with an Ekman pumping, while subsurface forcing, provided by smaller scale activity will be considered small. Thus subsurface flow will be significantly different from zero only in regions where flow streamlines do not encounter boundaries unable to support boundary layers or, obviously, where they close in the interior. The results illustrated by RYa strictly apply to circulations that close in the interior of the ocean although eddy resolving general

circulation models (see Holland *et al.*, 1984) suggest that they may apply also to flows passing through boundary currents. Therefore we will develop examples with wind stress curl distributions that give circulations which close either in the interior or in the western boundary.

In section 3 we present only the results of calculations of the three-layer model and make some comments on the results of the continuous case. In section 4 the homogeneous and two-layer model are considered for the ridge-like topography. Finally, in section 5 we make some speculations on the characteristic transport expected in the internal jets we have predicted and the possible role of instabilities in models which include the effects of relative vorticity.

2. Two-layer model

Our analysis is based on a quasi-geostrophic, two-layer, model on a β-plane, with a wind stress applied at the top of the model ocean. In this section we consider a simple constant slope topography at the bottom of the lower layer. We will assume that the dominant internal nonconservative mechanism is lateral diffusion of potential vorticity (for a discussion of this choice see Rhines and Young (1982b)). If relative vorticity is neglected, lateral diffusion of potential vorticity is equal and opposite in the two layers and therefore gives no contribution to the vertically integrated flow. Therefore bottom friction (for example) is also needed in order to balance the overall input of vorticity but we will assume its effect to be negligibly small except in narrow regions.

The steady two-layer quasi-geostrophic equations are:

$$J(\psi_1, q_1) = \frac{f_0 W_e}{H_1} + R\nabla^2 q_1 \tag{2.1}$$

$$J(\psi_2, q_2) = R\nabla^2 q_2 - D\nabla^2 \psi_2, \tag{2.2}$$

with $D \ll Rf_0^2/(g'H_2) \ll \beta L$, and

$$q_1 = \beta y + \nabla^2 \psi_1 + \frac{f_0^2}{g' H_1}(\psi_2 - \psi_1)$$

$$q_2 = \beta y + \nabla^2 \psi_2 + \frac{f_0^2}{g' H_2}(\psi_1 - \psi_2) + \frac{f_0 h}{H_2}$$

$$g' = \frac{\rho_2 - \rho_1}{\rho_2} g$$

where H_1, H_2 are the average depths of the upper and lower layers respectively and h is the topography.

In the interior of a wind driven gyre the relative vorticity is negligible with respect to the planetary vorticity and the vortex stretching term, and so are all the nonconserva-

tive terms. If the barotropic transport equation is formed one obtains:

$$\beta(H_1 + H_2)\psi_{bx} = f_0 h_x \psi_{2y} - f_0 h_y \psi_{2x} + f_0 W_e \tag{2.3}$$

where

$$(H_1 + H_2)\psi_b = H_1\psi_1 + H_2\psi_2.$$

Unlike the cases analyzed by RYa and YR, when topography is present the barotropic transport cannot be calculated without solving for the lower layer flow. On the other hand, flow in the lower layer will be (to the order where relative vorticity and nonconservative terms can be neglected) along the contours of

$$\hat{q}_2 = \beta y + \frac{f_0 h}{H_2} + \frac{f_0^2}{g' H_1 H_2}(H_1 + H_2)\psi_b$$

i. e., $\psi_2 = F(\hat{q}_2)$ and in particular $0 = F(\beta y + f_0 h/H_2)$ at the boundaries. In general the argument of the r.h.s. will not be constant on the boundaries and the only solution is the trivial one $F(\hat{q}_2) = 0$. This reasoning cannot be applied when the flow lines close either in the interior or in some boundary layer region, which we choose according to the dynamics of the specific problem. For example if topography is taken to be a constant, say positive, east-west slope ($h = h_x(x - x_e)$) we know that linear frictional boundary layers will be allowed on the northern side of the basin, in addition to the western one. In this case ψ_2 need not be zero if contours hit only the western or the northern boundaries, or obviously if they close upon themselves.

Throughout this section topography has in fact been chosen as a constant positive east-west slope, a ridge-like topography is dealt with in section 4. If such a slope is chosen to be of the same order as the β-term $\hat{q}_2$, contours would go across the basin in diagonal straight lines were it not for the interface displacement due to motion in the upper forced layer. If this forcing is weak, though, such modifications will be small and we can foresee that the lower layer flow will be zero. On the other hand if such an interface displacement becomes comparable to the β-effect (or the topographic term) there may be some regions where $\hat{q}_2$ contours are bent enough to allow flow in the lower layer.

To keep the mathematics as simple as possible we will select the forcing function in the form of (see Fig. 1)

$$\begin{aligned} W_e(x, y) &= Wf(y) \qquad W < 0 \\ f(y) &= \begin{cases} y/y_0 & \text{if } y < y_0 \\ 2 - y/y_0 & \text{if } y_0 \le y \le 3y_0 \\ y/y_0 - 4 & \text{if } 3y_0 \le y \le 4y_0 \end{cases} \end{aligned} \tag{2.4}$$

which in the absence of topography would give two gyres antisymmetric about the latitude of zero Ekman pumping.

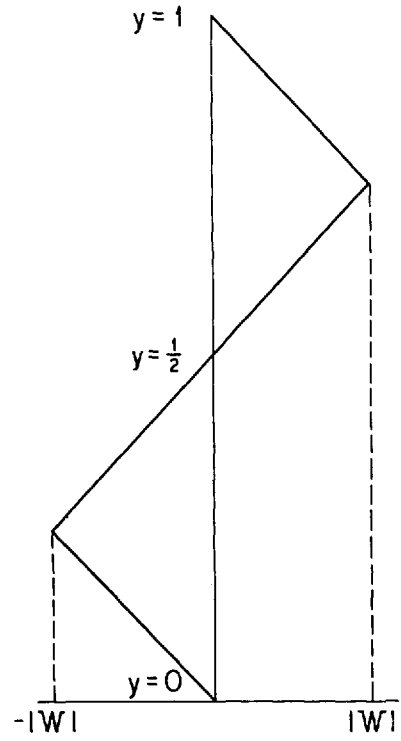

Figure 1. The Ekman pumping (2.4) as a function of latitude. The ordinate is $y/4y_0$.

Wherever the lower layer is motionless the vertically integrated transport can be calculated as

$$(H_1 + H_2)\psi_b = H_1\psi_1 = f_0 W_e(y)(x - x_e).$$

The resulting $\hat{q}_2$ contours are

$$\hat{q}_2 = \beta y + \frac{f_0}{H_2}(x - x_e)\left(h_x + \frac{f_0^2 W_e(y)}{g' H_1 \beta}\right).$$

Some examples are shown in Figure 2 for different values of the forcing and of the topographic slope. Notice that there is a region where the isolines do not meet either the eastern or the southern boundaries (it is there that the lower layer will be moving) and that this region increases as the forcing gets stronger. Comparing with the corresponding case for flat bottom, it is evident that the line dividing the subtropical and subpolar gyre is greatly displaced from the line of zero Ekman pumping, being altogether absent for large bottom slope/forcing ratios. Analogously to YR, RYa and Pedlosky and Young (1983), we will assume that where the lower layer moves it will do

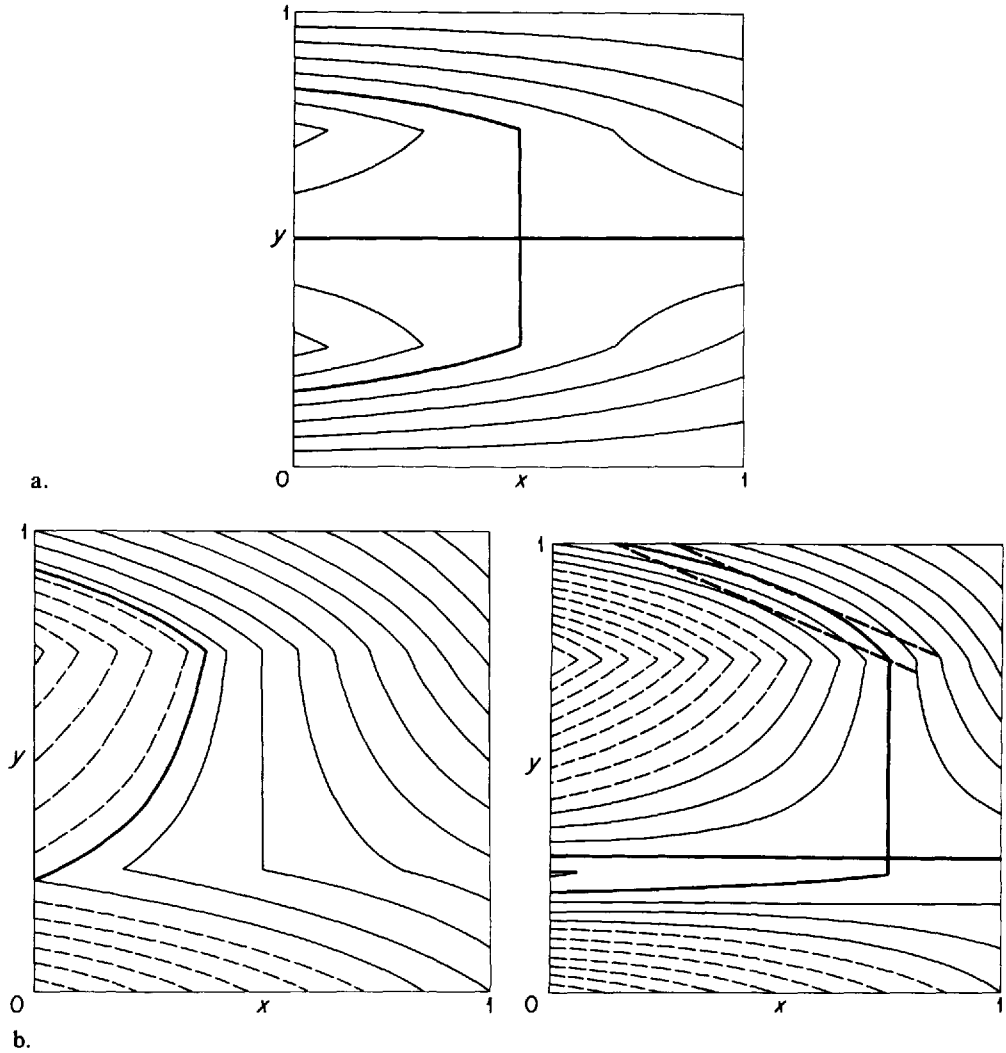

Figure 2. Isolines of $\hat{q}_2$ for the two-layer model in the nondimensional $x - y$ plane. Both x and y are scaled by x_e. (a)$H_1 = H_2, f_0 h_x/(\beta H_2) = 0, y_0/x_e = 1/4, f_0^3 W/(\beta^2 g' H_1 H_2) = -.5$ (b) same as for (a) except for $f_0 h_x/(\beta H_2) = .8$ (c) same as for (b) except for $f_0^3 W/(\beta^2 g' H_1 H_2) = -1.2$. The heavy line is the outermost closed $\hat{q}_2$ contour and the straight dashed lines are the characteristics (2.6).

so as to keep its potential vorticity constant. The arguments leading to the homogenization of potential vorticity may not hold when the flow lines pass through a viscous boundary layer (see Ierley and Young (1983)), they apply though when the flow lines close in the interior. Our point, however, is not to discuss here the validity of the homogenization arguments, and we hope to be able to convince the reader that our

results are independent of the choice of constant potential vorticity, although some details may change if a different choice is made.

In order to get closed $\hat{q}_2$ contours we must have:

$$x_e \frac{f_0^3 |W|}{g' H_1 H_2} > \beta^2 y_0. \tag{2.5}$$

Typical oceanic values are: $x_e = 6000$ km, $f_0 = 10^{-4}$ sec^{-1}, $H_1 = 1000$ m, $H_2 = 3000$ m, $\beta = 10^{-13}$cm^{-1} sec^{-1}, $y_0 = 1000$ km, $g' = 1$ cm/sec^2, $W = 10^{-4}$cm/sec. For these values the ratio of the left-hand side to the right-hand side of Eq. 2.5 is 2.

Furthermore, in order to obtain an anticyclonic circulation (beside the cyclonic one) as shown in Figure 2c we must have:

$$x_e \frac{f_0^3 |W|}{g' H_1 H_2} > \beta f_0 h_x y_0 / H_2.$$

The constant value Q_2 of potential vorticity is chosen in such a way as to match the streamfunction ψ_2 on the outermost closed $\hat{q}_2$ contour.

$$Q_2 = \beta y + f_0 (h_x / H_2)(x - x_e) + f_0^2 / (g' H_2)(\psi_1 - \psi_2).$$

Using this relation to eliminate ψ_1, the barotropic transport equation becomes

$$\beta(H_1 + H_2)\psi_{2x} - f_0 h_x \psi_{2y} = f_0 W_e + \beta H_1 g' h_x / f_0$$

and is independent of the (constant) value of Q_2, which appears only in the boundary conditions.

If the streamfunction is nondimensionalized with

$$\psi_2 = (\beta x_e H_1 g' / f_0^2)\psi_2' \qquad (x, y) = x_e(x', y')$$

dropping the primes one gets (see also de Szoeke (1985)):

$$(1 + H_2/H_1)\psi_{2x} - \frac{f_0 h_x}{\beta H_1}\psi_{2y} = \frac{f_0^3 W_e}{\beta^2 g' H_1^2} + \frac{f_0 h_x}{\beta H_1}$$

with $\psi_2 = 0$ on $\hat{q}_2(x, y) = Q_2$ which is a partial differential equation whose characteristics are:

$$\xi = y + \frac{f_0 h_x}{\beta(H_1 + H_2)}(x - x_e). \tag{2.6}$$

In Figure 2c it is shown that the characteristics intersect twice the outermost closed $\hat{q}_2$ contour in a significant portion of its perimeter. If the choice is made of satisfying the boundary condition of no normal flow at the intersection lying at lower latitude, ψ_2 will have, in general, a value different from zero at the intersection at higher latitude.

The physical mechanism may be more easily understood if a simpler geometry is

analyzed. Consider the following forcing function (compare with RYa)

$$W_e = -\alpha x \qquad \text{if } x^2 + y^2 < r_0^2$$
$$W_e = 0 \qquad \text{if } x^2 + y^2 < r_0^2$$

with the domain of the basin being $-\infty < x < +\infty$.

The governing equations are (2.1) and (2.2). Where the lower layer is motionless (take $H_1 = H_2 = H$)

$$\beta\psi_1 = \frac{f_0\alpha}{2H}(x^2 + y^2 - r_0^2) \qquad \text{if } (x^2 + y^2) < r_0^2$$
$$\beta\psi_1 = 0 \qquad \text{if } (x^2 + y^2) > r_0^2$$

which is the equation of concentric circles centered at (0, 0) of maximum radius r_0. $\hat{q}_2$ contours then become

$$\hat{q}_2 = \beta y + \frac{f_0 h_x x}{H} - \frac{f_0^2\alpha}{2g'H^2\beta}(x^2 + y^2 - r_0^2) \qquad \text{if } (x^2 + y^2) < r_0^2$$
$$\hat{q}_2 = \beta y + \frac{f_0 h_x x}{H} \qquad \text{if } (x^2 + y^2) > r_0^2.$$

The first is an equation for arcs of circle. If the forcing is strong enough, i.e., $r_0 > [x_0^2 + y_0^2]^{1/2}$ with $x_0 = \beta g'Hh_x/(\alpha f_0^2)$ and $y_0 = \beta^2 g'H^2/(\alpha f_0^3)$, these arcs may close to full circles centered at (x_0, y_0) with maximum radius $r_1 = r_0 - [x_0^2 + y_0^2]^{1/2}$ (see Fig. 3). Notice that in the absence of topography $x_0 = 0$ and the circles are centered about $x = 0$ so that $\iint_A W_e da = 0$, where A is the area enclosed by any circle centered at $x = 0, y = y_0$. When topography is added this center is shifted toward one side of the basin so that the total input of vorticity is nonzero and cannot be balanced without appending boundary layers. If the lower layer potential vorticity is assumed constant inside these circles the total transport is governed by:

$$2\beta\psi_{2x} - \frac{f_0 h_x}{H}\psi_{2y} = -f_0\alpha x/H + \beta g'Hf_0h_x/(f_0^2H)$$

where the characteristics are the same as in Eq. (2.6). Again on the northwest half of the r_1 circle the value of ψ_2 as resulting from the interior dynamics will be different from zero. In the following we show that the mismatch does not depend on the choice of constant potential vorticity and would arise in any case as long as topography depends on x.

Now returning to the more general case, suppose the forcing is such that there is a contour of $\hat{q}_2$ which closes in the interior with $\hat{q}_2 = \beta y + f_0 h/H_2 + F\Psi$ (Ψ is the upper layer streamfunction calculated with no lower layer flow and $F = f_0^2(H_1 + H_2)/(g'H_1H_2)$): inside this contour $\psi_2 = G(q)$ where $q = \beta y + f_0 h/H_2 + F\psi_1$. Therefore the

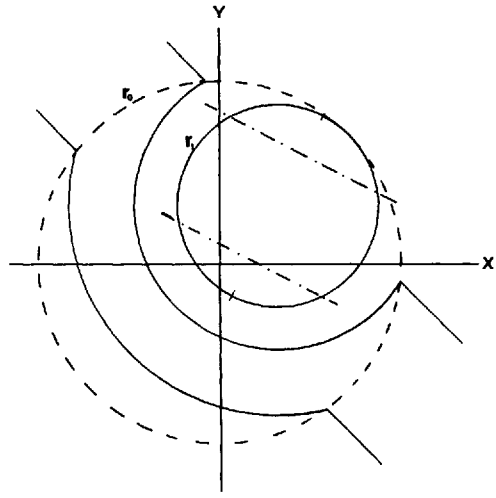

Figure 3. Contours of $\hat{q}_2$. The dashed circle ($r = r_0$) is the bounding contour for the barotropic streamfunction. The dashed-dot lines are the characteristics (2.6). On the northwest half of the outermost closed $\hat{q}_2$ contour ($r = r_1$) the value of ψ_2 will be different from zero.

equation for the vertically integrated transport in the presence of topography becomes (compare with Eq. 2.3):

$$\left(\beta + \frac{H_2}{H_1} F \frac{dG}{dq}\left(\beta + \frac{f_0 h_y}{H_2}\right)\right)\psi_{1x} - \frac{f_0 h_x}{H_1} F \frac{dG}{dq}\psi_{1y} = \frac{f_0 W_e}{H_1} = \beta \Psi_x.$$

We can change to a new coordinate system ξ and τ, where ξ are the characteristics of the flow, such that

$$\left(\beta + \frac{H_2}{H_1} F \frac{dG}{dq}\left(\beta + \frac{f_0 h_y}{H_2}\right)\right)\xi_x = \frac{f_0 h_x}{H_1} F \frac{dG}{dq}\xi_y$$

$$\frac{\partial x}{\partial \tau} = \beta + \frac{H_2}{H_1} F \frac{dG}{dq}\left(\beta + \frac{f_0 h_y}{H_2}\right)$$

$$\frac{\partial y}{\partial \tau} = -\frac{H_2}{H_1} F \frac{dG}{dq}\frac{f_0 h_x}{H_2}$$

so that the equation for ψ_1 becomes

$$\frac{\partial}{\partial \tau}\psi_1 = \beta \Psi_x.$$

We now integrate the equation along a line where ξ is constant ($\xi = \xi_0$) from the point τ_0 to the point τ_1, where τ_0 and τ_1 represent the intersections of $\xi = \xi_0$ with the

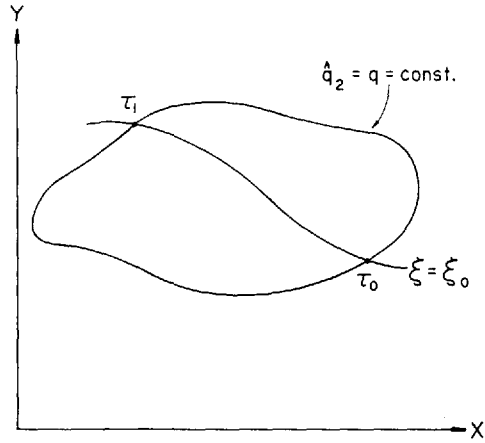

Figure 4. Sketch of the geometry for the integral constraints. See text for explanations.

outermost closed $\hat{q}_2$ contour, as schematically shown in Figure 4. Assuming that at τ_0 $\psi_1(\tau_0, \xi_0) = \Psi(\tau_0, \xi_0)$ we find

$$\psi_1(\tau_1, \xi_0) - \Psi(\tau_0, \xi_0) = \beta \int_{\tau_0}^{\tau_1} d\tau \frac{\partial}{\partial x} (\Psi(\xi_0, \tau))$$

$$\delta\psi_1 = \psi_1(\tau_1, \xi_0) - \Psi(\tau_1, \xi_0) = \beta \int_{\tau_0}^{\tau_1} d\tau \frac{\partial}{\partial x} (\Psi(\xi_0, \tau)) + \Psi(\tau_0, \xi_0) - \Psi(\tau_1, \xi_0).$$

Using the definition of $\hat{q}_2$

$$\Psi(\tau_0, \xi_0) - \Psi(\tau_1, \xi_0) = 1/F \int_{\tau_0}^{\tau_1} d\tau \frac{\partial}{\partial \tau} (\beta y + f_0 h/H_2 - \hat{q}_2)|_{\xi-\xi_0}$$

and recalling that $\hat{q}_2(\tau_0, \xi_0) = \hat{q}_2(\tau_1, \xi_0)$,

$$\delta\psi_1 = \beta \int_{\tau_0}^{\tau_1} d\tau \frac{\partial}{\partial x} (\Psi(\xi_0, \tau)) + 1/F \int_{\tau_0}^{\tau_1} d\tau \frac{\partial}{\partial \tau} (\beta y + f_0 h/H_2)|_{\xi-\xi_0}$$

and finally using the definition of τ

$$\delta\psi_1 = \psi_1(\tau_1, \xi_0) - \Psi(\tau_1, \xi_0) = \beta/F \int_{\tau_0}^{\tau_1} d\tau \, \hat{q}_{2x}.$$

The right-hand side vanishes for every value of ξ_0 only if τ = const. lines coincide with x = const. lines and this can only be if topography is independent of x. Similarly the jump in the lower layer is given by

$$\delta\psi_2 = \psi_2(\tau_1, \xi_0) = \beta \int_{\tau_0}^{\tau_1} d\tau \frac{dG}{dq} \hat{q}_{2x}.$$

Therefore, no matter what $G(q)$ will be, a mismatch in the streamfunction field will occur at the boundary of the region where the lower layer is moving. Because the existence of the mismatch is independent of the particular form of $G(q)$, we will continue our calculations making the convenient assumption that potential vorticity is constant in the lower layer. Notice that the jump in the lower layer potential vorticity q_2 is

$$q_2(\tau_1, \xi_0) - \hat{q}_2(\tau_1, \xi_0) = \beta \int_{\tau_0}^{\tau_1} d\tau \left(1 - F\frac{dG}{dq}\right)\hat{q}_{2x}$$

and for the abovementioned choice $dG/dq = 1/F$ so that there is no jump in potential vorticity. In Figure 5 the resulting streamlines for the two layers are shown for the more realistic wind stress pattern (2.4).

Because of the choice of constant potential vorticity the mismatch at the boundary of the outermost closed $\hat{q}_2$ contour is equal in the two layers. This is plausible since this choice implies strong interfacial friction which tightly locks the two layers. If for example bottom friction is considered of the same order as interfacial friction, the circulation integral inside closed $\hat{q}_2$ contours (see RYa) gives

$$q = F(1 + D/R)\psi_2 + \text{constant}$$

where D is the coefficient of bottom friction. Now the boundary layer transport in the upper layer will be larger than that in the lower layer, in particular

$$\delta\psi_1 = (1 + D/R)\delta\psi_2.$$

The position of the mismatch where a boundary layer has to be appended is consistent with the notion that in the presence of this topographic slope a barotropic flow would be able to form a linear viscous boundary layer on the northern side of the basin (see Appendix A). The length of the mismatch region increases with the topographic slope and the strength of the forcing (see Table 1a). From Eq. (A.3) it can be checked that as the point of maximum upwelling shifts northward the length of the mismatch region becomes larger. On the other hand if one considers a fixed distance on the outermost closed $\hat{q}_2$ contour from the point x_0 where the discontinuity begins, the strength of the jump is almost independent of the parameters. Because the jump increases with increasing distance from x_0 (see Table 1b), the final transport entering the western boundary will increase with the topographic slope and the forcing strength.

It is appropriate to mention here that the line of zero transport does not coincide in the two layers unlike the case for flat bottom. Moreover there is some vertically integrated flow across the line of zero Ekman pumping. When a subtropical gyre appears in the lower layer (see Fig. 5b) the flow tends to be rather zonal in the southwest corner of the subpolar gyre, in close analogy to the case of a barotropic flow in the presence of the same topography (see Appendix B and Fig. B1). As could have

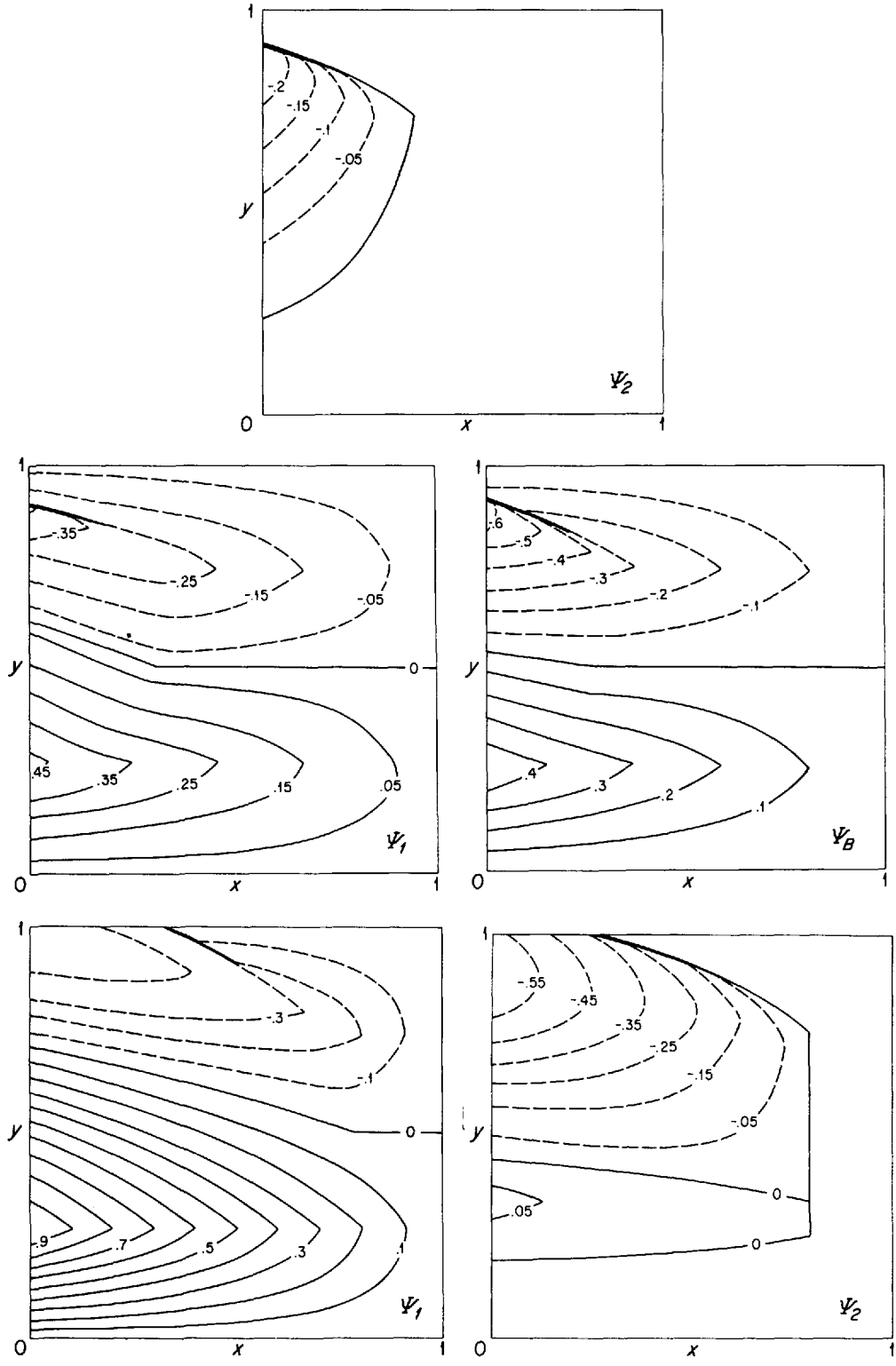

Figure 5. Streamlines for the flow in the two-layer model. (a) $f_0^3 W/(\beta^2 g' H_1 H_2) = -.5$; (b) $f_0^3 W/(\beta^2 g' H_1 H_2) = -1.2$. The line of increasing thickness shows the location of the discontinuity.

Table 1a. Easternmost point of discontinuity in units of x_e (constant slope topography) as a function of the nondimensional forcing $f_0^3 W/(\beta^2 g' H_1^2)$ (rows) and topographic slope $f_0 h_x/(\beta H_2)$ (columns).

	Topographic slope				
Forcing	.4	.8	1.2	1.6	2.0
−.50	.000	.154	.193	.213	.225
−.75	.203	.390	.390	.390	.390
−1.00	.315	.500	.528	.510	.500
−1.25	.388	.560	.628	.604	.584
−1.50	.440	.601	.667	.684	.653
−1.75	.480	.663	.695	.729	.714
−2.00	.513	.657	.717	.750	.780

been expected, when the forcing gets stronger the circulation in the lower layer resembles more closely the forcing pattern itself and, therefore, the flat bottom circulation. Comparing the lower layer streamfunctions of Figures 5a and 5b it can be seen that the water crossing the zero Ekman pumping line (at $y = 1/2$) is of a more southern origin when the forcing is weaker.

We now want to increase the vertical resolution of our model in order to test the robustness of our results and to see whether topography produces other new features when more layers are added.

3. Three-layer model

In order to make useful comparison between the two- and three-layer model, we have to choose our parameters in such a way that these models represent different approximations of the same physical process. Therefore some minimal requirements arise: the total mass of our system has to be the same and the mass of cold and warm waters have to be separately conserved. The first statement implies that, to the order considered by the Boussinesq approximation the total volume has to be the same in the two models. Therefore, indicating the two-layer model variables with primes

$$H_1 + H_2 + H_3 = H_1' + H_2' = 2H \text{ for equal layers.}$$

Table 1b. Transport of lower layer flow at the northern boundary of closed $\hat{q}_2$ contours, as a function of the distance from the point x_0/x_e where the discontinuity begins (columns), for two values of the forcing $f_0^3 W/(\beta^2 g' H_1^2)$ (rows), with slope $f_0 h_x/(\beta H_2) = .8$.

	Distance from X_0							
Forcing	.05	.10	.15	.20	.25	.30	.35	.40
−1.25	−.03	−.07	−.11	−.16	−.21	−.26	−.32	−.38
−1.75	−.02	−.06	−.11	−.16	−.21	−.27	−.35	−.43

The second statement is not as easy to quantify, but a simple formulation which clearly satisfies it is:

$$\rho_1' = \rho_1; \quad H_1' = H_1; \quad \rho_2 H_2 + \rho_3 H_3 = \rho_2' H_2'$$

which gives

$$g'(H_1 + H_3) + g'' H_3 = g_1' H \tag{3.1}$$

where $g' = (\rho_2 - \rho_1)g/\rho_2$, $g'' = (\rho_3 - \rho_2)g/\rho_2$, $g_1' = (\rho_2' - \rho_1')g/\rho_1'$.

The equations for a quasi-geostrophic, very large-scale, β-plane, steady three-layer model in the presence of wind stress forcing, bottom topography, small lateral diffusion of potential vorticity and very small bottom friction, are:

$$\begin{aligned}
J(\psi_1, q_1) &= \frac{f_0 W_e}{H_1} + R\nabla^2 q_1 \\
J(\psi_2, q_2) &= R\nabla^2 q_2 \\
J(\psi_3, q_3) &= R\nabla^2 q_3 - D\nabla^2 \psi_3, \\
q_1 &= \beta y + \frac{f_0^2}{g' H_1}(\psi_2 - \psi_1) \\
q_2 &= \beta y + \frac{f_0^2}{g' H_2}(\psi_1 - \psi_2) + \frac{f_0^2}{g'' H_2}(\psi_3 - \psi_2) \\
q_3 &= \beta y + \frac{f_0^2}{g'' H_3}(\psi_2 - \psi_3) + \frac{f_0 h}{H_3}.
\end{aligned}$$

Again we will assume that the potential vorticity is constant in the two unforced layers, in those regions where the streamlines do not hit either the eastern or the southern boundaries. The limiting contours of such regions are again found assuming no flow in each layer outside them and are shown in Figures 6a and 6b. Now the condition on the forcing strength in order to have a deep moving layer is:

$$x_e \frac{f_0^3 |W|}{g_1' H^2} > \gamma \beta^2 y_0$$

with

$$\gamma = \frac{H_3 H_2}{H H_1} \frac{g''}{g_1'} + \frac{H_3}{H} \frac{(g' + g'')}{g_1'} + \frac{g'}{g_1'} \frac{H_2}{H}$$

and the analogous condition for the middle layer is:

$$x_e \frac{f_0^3 |W|}{g_1' H^2} > \frac{g'}{g_1'} \frac{H_2}{H} \beta^2 y_0.$$

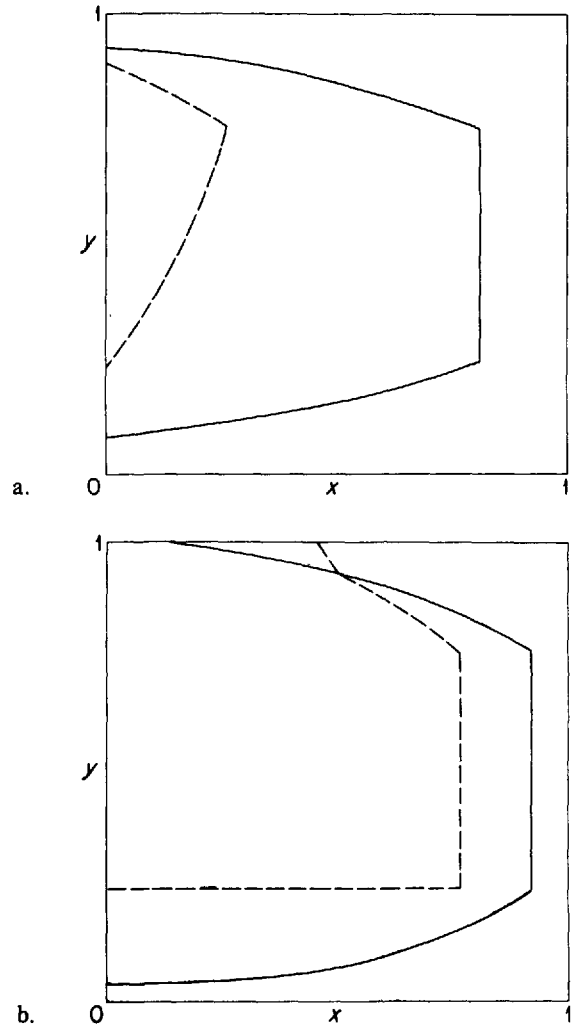

Figure 6. Bounding contours for the regions of flow in the middle and lowest layer. Outside the dashed line $\psi_3 = 0$. Outside the full line $\psi_2 = 0$. (a) $f_0 h_x/(\beta H_1) = .8$, $y_0/x_e = 1/4$, $H_1 = D$, $f_0^3 W/(\beta^2 g' H_1^2) = -.5$, $g'/g_1' = 3/4$, $g''/g_1' = 1/2$, $H_2/D = H_3/D = 1/2$. (b) same as for (a) except for $f_0^3 W/(\beta^2 g' H_1^2) = -1.2$.

Notice that, because of our choice (3.1), in order for the deepest layer to move the forcing has to be stronger than in the equivalent situation for two layers. In particular

$$x_e \frac{f_0^3 |W|}{g_1' H^2} > (1 + H_3 H_2 g''/(H^2 g_1'))\beta^2 y_0$$

which is to be compared with Eq. (2.5).

In the following we will present the results without showing the detailed derivation, emphasizing the similarities with the two-layer model and the new findings for increased vertical resolution.

One result of the introduction of bottom topography can be readily seen by inspection of Figure 6b: there is a small region at the northwest corner of the basin where the deepest layer moves although the middle layer does not. This is quite contrary to the results in the absence of topography where the region of "closed q_3 contours is properly contained in the region of closed q_2 contours" (see RYa). This lack of "nesting" of the closed q contours also occurs when ventilation is present (see LPS) although for different reasons. In the calculations we have done, though, we haven't corrected the lowest layer flow for the absence of motion in the middle layer, since this region is very small.

In the region where all layers are moving the characteristics of the equation for the vertically integrated transport are the same as in the two-layer model (Eq. 2.6). Therefore the characteristic lines are independent of the stratification.

In Figure 7 an example of flow is shown for one value of the forcing strength. Notice that, as in the two-layer case, the line of zero transport is different in each layer, except, of course, in the region where topography is not felt. Again in all layers there will be noticeable exchange of water across the zero Ekman pumping line, a feature which is absent in the flat bottom model. Although the small region where $\psi_2 = 0$ and $\psi_3 \neq 0$ is not shown we have checked that the mismatch at the southern side of its limiting contour where ψ_2 and ψ_3 become nonzero, still exist together with a nonzero flow at the northern rigid boundary.

We have extended these calculations to a continuously stratified model, again assuming constant potential vorticity inside the region containing the subsurface flow. In particular at the bottom, the quantity which is conserved is $(f_0/N^2)(\partial\psi/\partial z) + h$ (N is the Brunt-Väisälä frequency), which can be thought of as bottom layer potential vorticity in the limit of vanishing layer thickness. Similarly to the three-layer model, there is a region at the northwest corner of the basin where the bottom water moves (as well as the surface water) although there is no flow at mid-depth. Again in the region where the water moves top to bottom, the characteristics of the equation governing the vertically integrated flow are given by Eq. 2.6.

4. Ridge-like topography

In this section we analyze the effects of a bottom topography of varying slope on both a barotropic and a two-layer model on a β-plane. Topography will be ridge-like, i.e.,

$$h = \begin{cases} -h_x|x - x_0| + h_x a & \text{for } |x - x_0| < a \\ 0 & \text{for } |x - x_0| > a \end{cases}$$

where x_0 is the point of maximum height $h_x a$, and a is the halfwidth of the ridge. First consider the case of one layer forced by a wind stress curl which is always negative, for

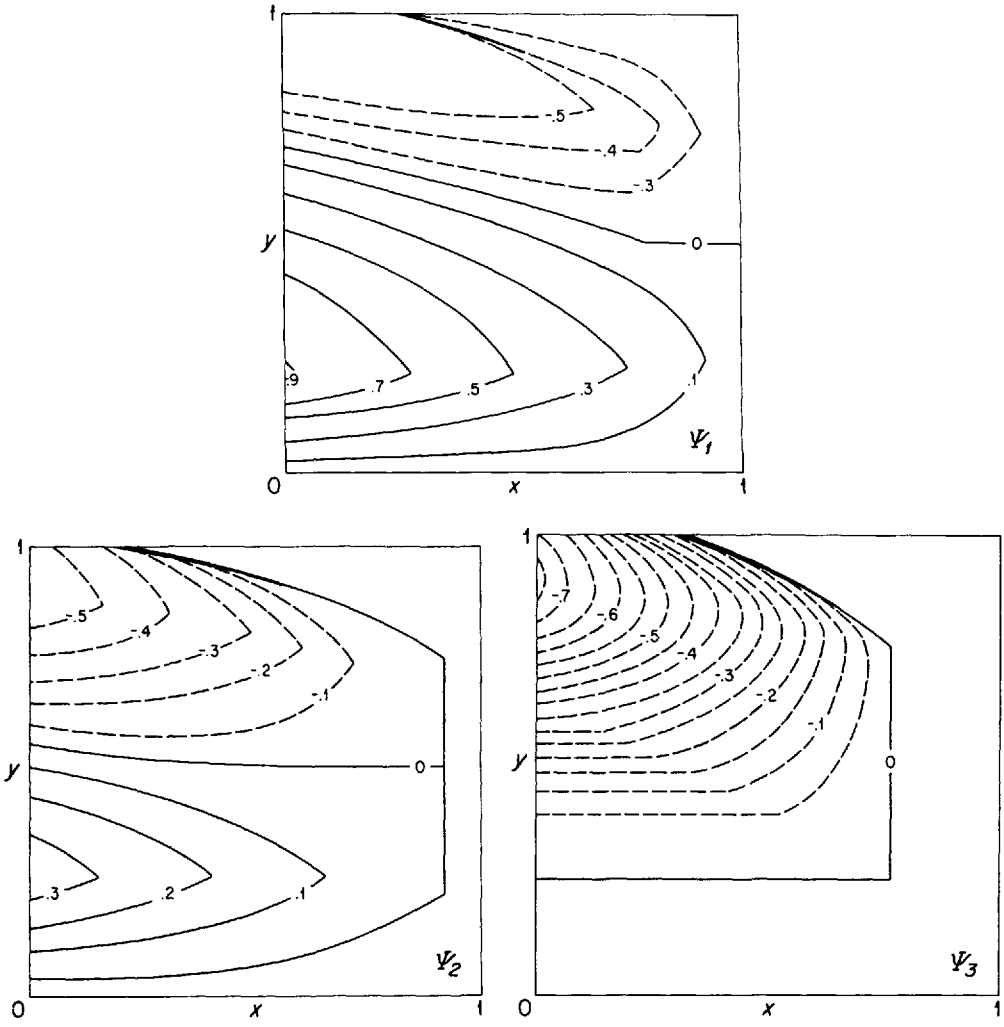

Figure 7. Streamlines for the three-layer model. Same parameters as in Figure 6b. The line of increasing thickness shows the location of the discontinuity.

example that of Eq. 2.4 with y between 0 and y_0. The equation governing the flow will be

$$J(\psi_1, \beta y + f_0 h/H) = f_0 W_e(y)/H\,. \tag{4.1}$$

The characteristics of the flow will be the geostrophic contours $\xi = \beta y + f_0 h/H$, which are piecewise continuous broken lines dividing the domain in 8 different regions (see Fig 8). If we require the flow to be zero at the eastern boundary and at the zeroes of the

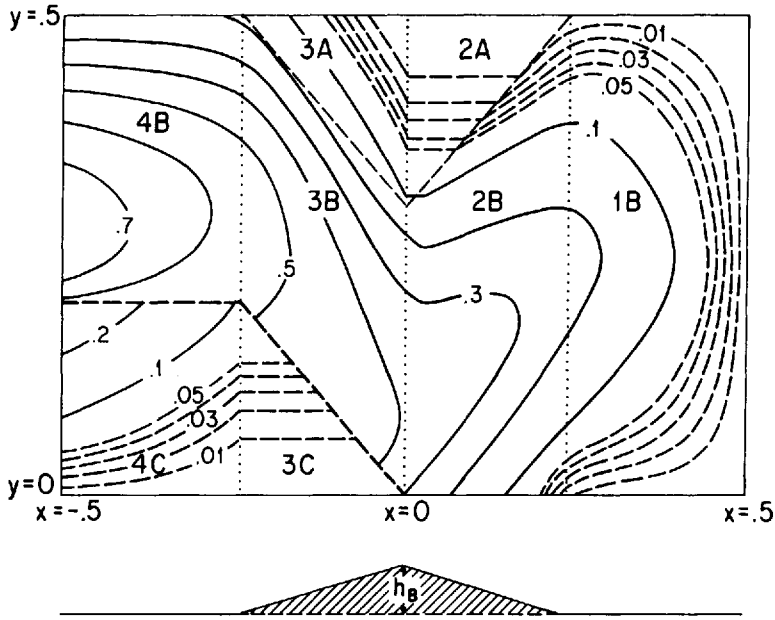

Figure 8. Streamlines for the flow of the barotropic model in the presence of ridge-like topography. The thin dashed line represents one of the characteristics dividing the domain in different regions. The thick dashed line represents the characteristic at the location of the discontinuity.

Ekman pumping we obtain the following results for the streamfunction for the different regions shown in Figure 8.

$$(1B)\quad \psi_1 = f_0 W_e(y)(x - x_e)/(\beta H)$$

$$(2B)\quad \psi_1 = \frac{1}{h_x}\int_{\xi/\beta}^{y} d\eta\, W_e(\eta) + f_0 W_e(\xi/\beta)(x_0 + a - x_e)/(\beta H)$$

$$(2A)\quad \psi_1 = \frac{1}{h_x}\int_{0}^{y} d\eta\, W_e(\eta)$$

$$(3C)\quad \psi_1 = -\frac{1}{h_x}\int_{0}^{y} d\eta\, W_e(\eta)$$

$$(3A)\quad \psi_1 = -\frac{1}{h_x}\int_{s(\xi)}^{y} d\eta\, W_e(\eta) + 1/h_x \int_{2y_0}^{s(\xi)} d\eta\, W_e(\eta)$$

$$(3B)\quad \psi_1 = -\frac{1}{h_x}\int_{s(\xi)}^{y} d\eta\, W_e(\eta) + 1/h_x \int_{2y_0}^{s(\xi)} d\eta\, W_e(\eta) + f_0 W_e(\xi/\beta)(x_0 - a - x_e)/(\beta H)$$

$$(4C)\quad \psi_1 = -\frac{1}{h_x}\int_0^y d\eta\, W_e(\eta) + f_0 W_e(y)(x - x_e + a)/(\beta H)$$

$$(4B)\quad \psi_1 = -\frac{2}{h_x}\int_{s(\beta y)}^y d\eta\, W_e(\eta) + f_0 W_e(y)(x - x_e + 2a)/(\beta H)$$

where $s(\xi) = \xi/\beta - f_0 h_x a/(\beta H)$.

Notice that the flow in regions 2A and 3C is perfectly zonal and a discontinuity arises at the boundary between regions C and B, in addition to discontinuities at the western and parts of the northern and southern boundaries. The difference in transport between regions B andC is given by

$$\begin{aligned} T_{B-C} &= [\psi_1(3B) - \psi_1(3C)]_{\xi - f_0 h_x a/(\beta H)} \\ &= f_0^2 W h_x a(x_0 + a/2 - x_e)/(\beta^2 y_0 H) \end{aligned}$$

and is constant.

The physical mechanism of this discontinuity can be understood by means of the following analogy. Eq. 4.1 is equivalent to the equation for the concentration of a passive tracer advected by a known velocity field (here the concentration is analogous to ψ_1 and the known velocity field has flow lines identical to the geostrophic contours ξ).

In the absence of forcing and dissipation the concentration will be constant along the flow lines and will be completely determined by the knowledge of the concentration at the boundaries of the domain under consideration. On the other hand, there might be some regions in the interior of the domain (such as the line dividing regions C and B in Fig. 8) where neighboring flow lines trace back to regions of the boundaries that are very far apart and thus might have rather different concentration values. Therefore although the concentration is continuous along the boundary it may become discontinuous in the interior.

This explains also why in our oceanic, wind-forced problem the jump in transport across the discontinuity is constant. In the presence of forcing the flow is the sum of two components: one across and the other along the geostrophic contours. The former is determined by the forcing and is continuous on the characteristic dividing regions C and B as long as the forcing is continuous there. The discontinuity arises in the component along the characteristics (the only one in the passive tracer analogue) which is obviously constant on a characteristic.

To emphasize the dependence upon the parameters we notice that the transport across the discontinuity can be written as

$$T_{B-C} = T_s \frac{\Delta h/H}{\Delta f/f_0} \frac{(x_0 + a/2 - x_e)}{x_e}$$

where $T_s = f_0 W x_e/\beta$ is the maximum Sverdrup transport in the absence of topography, $\Delta h/H = h_x a/H$ is the relative change in height due to the topography and

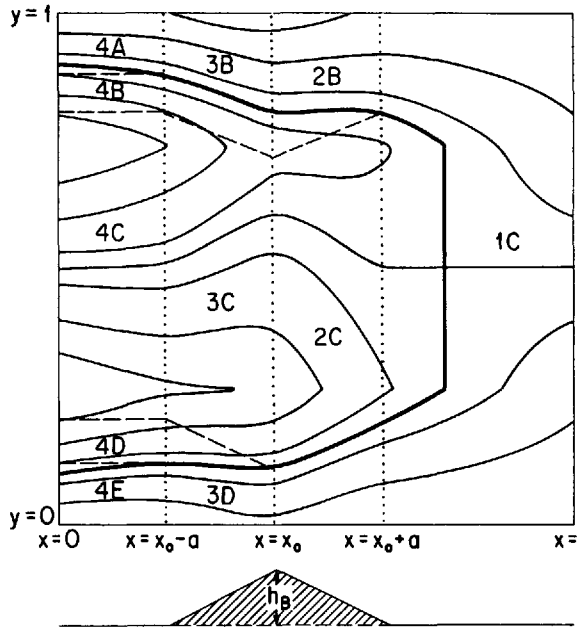

Figure 9. Contours of $\hat{q}_2$. The heavy line represents the outermost closed contour and the dashed lines are the characteristics dividing the domain in different regions. $f_0^3 W/(\beta^2 g' H_1^2) = -1.$, $f_0 h_x/(\beta H_2) = .8$, $x_0/x_e = .4$, $a/x_e = .2$.

$\Delta f/f_0 = \beta y_0/f_0$ is the characteristic change in Coriolis parameter. For $x_e = 6000$ km, $f_0 = 10^{-4}$ sec^{-1}, $W = 10^{-4}$ cm/sec, $y_0 = 1000$ km, $H = 4000$ m, $\beta = 10^{-13}$ cm^{-1}/sec^{-1}, $\Delta h = 1000$ m, $x_0 = 3000$ km, $a = 1200$ km, $T_s = 60$ Sv we get $T_{B-C} = 60$ Sv. This value is clearly an upper limit for the transport at the jump since the barotropic model velocities are very large at the bottom. Also the ridge height and the basin width are very large in this example, at the limit of applicability of the quasi-geostrophic approximation. Nevertheless this value is indicative of the fact that these jets have transport of the same order as the interior flow.

We now want to see what are the effects of this ridge-like topography on the two layers model considered in section 1. Again the forcing will be that of Figure 1. We will take the streamfunction in the lower layer such as to keep q_2 constant inside the outermost closed $\hat{q}_2$ contour and ψ_2 zero outside where now

$$\hat{q}_2 = \beta y + \frac{f_0 h_x}{H_2}(-|x - x_0| + a) + (x - x_e)\frac{f_0^3 W_e(y)}{\beta g' H_1 H_2}$$

an example is given in Figure 9. The characteristics of the flow will be

$$\xi = \beta y + f_0 h/(H_1 + H_2)$$

Table 2. Difference in transport (ridge-like topography) in the lower layer at the northern jump (region 4B – 4A) for different values of the slope $f_0 h_x/(\beta H_2)$ (columns), and the ridge halfwidth a/x_e (rows). (a) $f_0^3 W/(\beta^2 g' H_1^2) = -1.0$; (b) $f_0^3 W/(\beta^2 g' H_1^2) = -2.0$.

a.

Ridge halfwidth	Topographic slope .4	.8	1.2	1.6	2.0
0.1	−.04	−.07	−.09	−.10	−.11
0.2	−.09	−.14	−.18	−.22	−.25
0.3	−.14	−.22	−.28	−.34	−.37

b.

Ridge halfwidth	Topographic slope .4	.8	1.2	1.6	2.0
0.1	−.06	−.08	−.10	−.11	−.12
0.2	−.12	−.18	−.22	−.27	−.30
0.3	−.18	−.29	−.39	−.45	−.47
0.4	−.26	−.43	−.56	−.58	−.56

and they divide the region of lower layer flow in several parts shown in Figure 9. Similarly to the barotropic case, in the lower layer there are two regions of weak quasi-zonal flow (2B and 3D in Fig. 9) and a discontinuity in flow between regions C and D. The jump in the streamfunction is the same in the two layers because of the choice of constant potential vorticity. The vertically integrated difference in transport at the jump is given by

$$T_{C\text{-}D} = \frac{f_0 h_x a}{\beta(H_1+H_2)} [g'\beta H_1 H_2/f_0^2 + f_0 W(x_0 + a/2 - x_e)/(\beta y_0)]$$

and is always larger than the corresponding value for the one-layer model. A mismatch analogous to that of section 1 occurs at the northern boundary of region 3B inducing a discontinuity which continues with constant value at the boundary between regions 4A and 4B. In Table 2 some values for this jump in the lower-layer streamfunction are given for different values of the topographic slope, the width of the ridge and the strength of the forcing. The nondimensional slope $f_0 h_x/(\beta H) = 2.$ and the nondimensional halfwidth $a/x_e = .2$ in Table 2a correspond to the dimensional values given in the previous example for the homogeneous model. This gives a dimensional total transport of 60 Sv, which fortuitously happens to be the same value as the internal jet transport for the barotropic model, and again this value is comparable to the interior transport. Notice that this discontinuity grows more slowly with the topographic slope than $T_{C\text{-}D}$, while doubling the width of the ridge more than doubles the amplitude of the discontinuity. This is what one would actually expect since the "internal" jump (C – D) owes its existence to the change in slope of the bottom topography. In fact

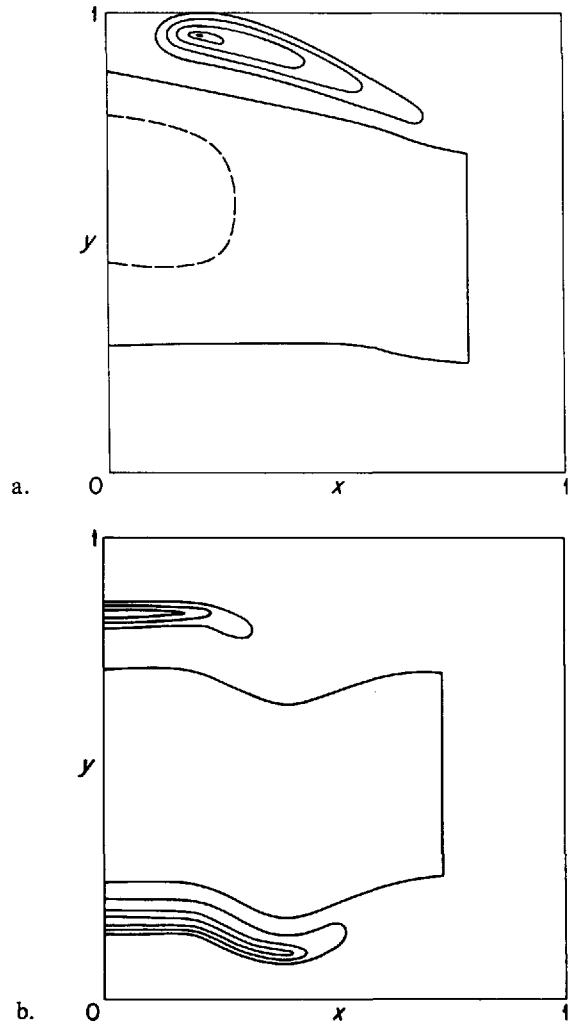

Figure 10. Contours of the zonal velocity field in the lower layer. Contours are smoothed since velocity is computed with finite difference from the streamline field. (Full line for negative values.) (a) Constant slope topography. $f_0^3 W/(\beta^2 g' H_1 H_2) = -1.$, all the other parameters as in Figure 5b. (b) Ridge-like topography. All parameters as in Figure 9.

taking a very thin ridge, but with constant height ($h_x a$ = constant, $a \to 0$) the internal jump would continue to exist with almost unchanged strength while the mismatch at the northern boundary of region 3B tends to vanish. For reasonable values of the parameters both these discontinuities are of the same magnitude as the interior flow and they arise in regions away (although connected to) the solid boundaries of the domain.

5. Discussion

We have shown how in the presence of topography internal jets arise when simple Sverdrup dynamics are used. More specifically we find that for baroclinic gyres, jets are formed at the boundary of the region containing the subsurface flow. Their existence is independent of the forcing mechanism for the lower layer as long as such forcing is small. On the other hand their very presence raises questions about the applicability of conservative dynamics since at the jets' locations frictional effects have to be much stronger than we considered initially. To avoid such difficulties de Szoeke (1985), in an independent work on the same subject, has chosen to prescribe the flow as completely continuous in both layers. This choice implies that either the forcing has to be of a special form or that the eastern boundary condition cannot be applied in the upper layer. We think, however, that it is inescapable to embed the circulation in a closed basin and the occurrence of flows with internal jets must not be ruled out *a priori*.

Since our results are not sensitive to the choice of constant potential vorticity in the lower layer we need not restrict ourselves to constant slope topography. Therefore we have also analyzed the effects of bottom topography of varying slope, in particular in the form of a ridge. Again jets are found although of a different nature. In fact in this case, internal jets occur in both stratified and even in homogeneous models; their existence now is due to the change in sign of the bottom slope and the presence of the southern gyre boundary along which ψ vanishes. For values of the parameters in the oceanic range, the jets produced both in the ridge-like and in the constant slope topography have very large transports, i.e. on the order of the maximum transport of the interior flow. Notice also that for the choice of constant potential vorticity in the subsurface layers all the internal jets occurring both in the constant slope and in the ridge-like topography are westward (see Fig. 10) and they would be so even if the slope were of the opposite sign. Therefore, if unstable, they could radiate to the interior of the ocean where eddy energy is observed.

It is our intention in the future to examine numerical models that include relative vorticity and small nonconservative mechanisms to see whether the features found in the previous sections actually occur. It is possible that internal dynamics adjust the flow so that the strong internal jets obtained with simple Sverdrup relation are avoided. This would imply a deep modification of the vorticity balance which would be worth analyzing.

Acknowledgments. PC wishes to thank Drs. Anna Trevisan, Andrea Buzzi and Piero Malguzzi for helpful discussions and for providing an office and computer facilities. This research was carried out at the University of Bologna (Italy) where PC was supported by her parents. Partial support by NSF Grant OCE-8214821 is also acknowledged. JP is supported by a grant from the National Science Foundation's Division of Atmospheric Sciences. This is contribution number 6090 of the Woods Hole Oceanographic Institution.

APPENDIX A

Assuming that lower layer potential vorticity is constant in the boundary layer, the equation for the barotropic flow in the presence of small bottom friction is:

$$(1 + H_2/H_1)\psi_{2x} - \frac{f_0 h_x}{\beta H_1}\psi_{2y} = \frac{f_0^3 W_e}{\beta^2 g' H_1^2} + \frac{f_0 h_x}{\beta H_1} - \frac{DH_2}{\beta L H_1}\nabla^2\psi_2.$$

The boundary of validity of constant potential vorticity dynamics is

$$Q_2/\beta = y + f_0 h_x(x - x_e)/(\beta H_2) + f_0^3 W f(y)(x - x_e)/(g'\beta^2 H_2 H_1).$$

Therefore, we define as boundary layer variable

$$\epsilon\xi = y + (x - x_e)(r + w_0 f(y)) - Q_2/\beta$$

where $r = f_0 h_x/(\beta H_2)$, $w_0 = f_0^3 W/(\beta^2 g' H_1 H_2)$;

and $\lambda = x - x_e$ as the other independent variable.

The dominant balance is (for $\epsilon = DH_2/(\beta L H_1)$):

$$c(\lambda)\frac{\partial\psi_2}{\partial\xi} + g(\lambda)\frac{\partial^2\psi_2}{\partial\xi^2} = 0$$

where $g(\lambda)$ is always positive:

$$g(\lambda) = \left[\frac{r + 4w_0(Q_2/\beta - 1)}{1 + 4w_0\lambda}\right]^2 + (1 + 4w_0\lambda)^2$$

and

$$c(\lambda) = \frac{2[r + 4w_0(Q_2/\beta - 1)] - r(1 + 4w_0\lambda)^2}{1 + 4w_0\lambda}.$$

In order to get solutions which are decaying for $\xi \to -\infty$ (inside the region of constant potential vorticity) we must have $c(\lambda) < 0$, which gives:

$$\lambda < [1 - \sqrt{2 + 8w_0(Q_2/\beta - 1)/r}]/(4|w_0|). \tag{A.1}$$

This is exactly the relation which determines the point at which the boundary is tangent to the characteristics. For $x - x_e$ greater than this value the boundary layer streamfunction grows exponentially but the amplitude of the boundary layer correction goes to zero.

$$\psi_2(\xi, \lambda) = A(\lambda)[1 - \exp(-g(\lambda)\xi/c(\lambda))]$$

where $A(\lambda) = -2w_0(Y - Y_s)(Y + Y_s - 2 + r/(2w_0))/r$

with $Y = (Q_2/\beta - r\lambda + 4w_0\lambda)/(1 + 4w_0\lambda)$

and $Y_s = r\lambda/2 + 1 - r/(8w_0)$.

At the point given by (A.1) $Y = Y_s$ and $A(\lambda) = 0$.

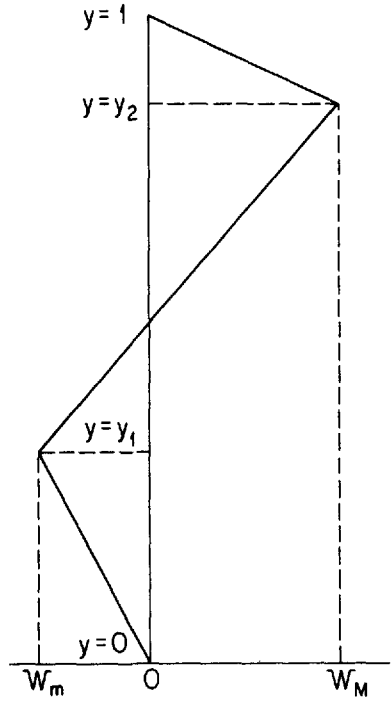

Figure A1. The Ekman pumping (A.2) as a function of y.

If the Ekman pumping is taken of a more general form (see Fig. A1) (here the variables are nondimensional):

$$w(y) = \begin{cases} w_{0m} y / y_1 & \text{if } y < y_1 \\ \dfrac{(w_{0M} - w_{0m}) y + y_2 w_{0m} - y_1 w_{0M}}{y_2 - y_1} & \text{if } y_1 \le y \le y_2 \\ w_{0M}(y - 1)/(y_2 - 1) & \text{if } y_2 \le y \le 1. \end{cases} \tag{A.2}$$

The point at which the outermost closed q_2 contour is tangent to the characteristics is:

$$\lambda = (y_2 - 1)(2b - 1)/w_{0M} \tag{A.3}$$

where

$$b = \left[\frac{(1 + w_{0M}/r)[w_M(1 - y_1) - w_{0m}(1 - y_2)]}{2(1 - y_2)(w_{0M} - w_{0m})} \right].$$

APPENDIX B

The equation governing the transport of one layer of homogeneous fluid in the presence of topography $h = \alpha x$, forced by a longitude independent Ekman pumping

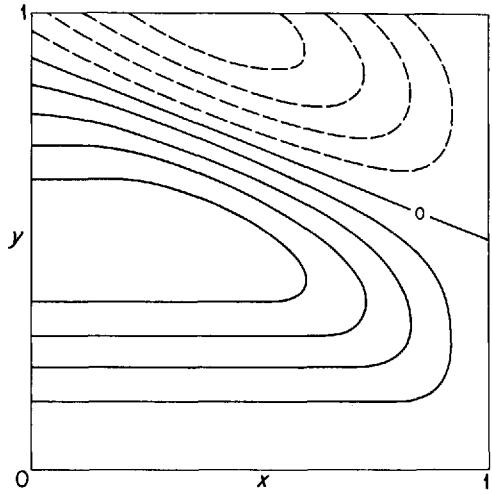

Figure B2. Streamlines for the barotropic streamfunction resulting from the Ekman pumping $W_e = W \sin(2\pi y)$. With $f_0^3 W/(\beta^2 g H^2) = -1.2$ and $f_0\alpha/(\beta H) = .8$.

is:

$$\beta\psi_{bx} - f_0\alpha/H\,\psi_{by} = f_0 W_e(y)/H.$$

Setting $\xi = y + f_0\alpha(x - x_e)/(\beta H) = y + r(x - x_e)$ its solution is:

$$\psi_b = -\int^y d\eta W_e/\alpha + \phi(\xi).$$

Given the form and the modified β-effect we choose to satisfy the following boundary conditions:

$$\psi_b = 0 \text{ on } x = x_e \quad \text{and} \quad \psi_b = 0 \text{ on } y = 0.$$

Therefore the flow is divided into regimes:

$$\psi_b = -\int_{y+r(x-x_e)}^{y} d\eta W_e/\alpha \quad \text{for } \xi > 0$$

and

$$\psi_b = -\int_0^y d\eta W_e/\alpha \quad \text{for } \xi < 0.$$

Because of the choice of an x-independent forcing, in the southwest part of the basin the flow is perfectly zonal. Notice also how the cyclonic gyre is reduced in favor of the subtropical gyre (see Fig. B1).

REFERENCES

de Szoeke, R. A. 1985. Wind-driven mid-ocean baroclinic gyres over topography; extension of the Sverdrup relation. J. Mar. Res., *43,* 793–824.

Holland, W. R., T. Keffer and P. B. Rhines. 1984. Dynamics of the oceanic general circulation: the potential vorticity field. Nature, *308,* 698–704.

Ierley, G. R. and W. R. Young. 1983. Can the western boundary layer affect the potential vorticity distribution in the Sverdrup interior of a wind gyre?. J. Phys. Oceanogr., *13,* 1753–1763.

Luyten, J. L., J. Pedlosky and H. Stommel. 1983. The ventilated thermocline. J Phys. Oceanogr., *13,* 292–309.

Luyten, J. L., H. Stommel and C. I. Wunsch. 1985. A diagnostic study of the Northern Atlantic subpolar gyre. J. Phys. Oceanogr., *15,* 1344–1358.

Pedlosky, J. and W. R. Young. 1983. Ventilation, potential vorticity homogenization and the structure of the ocean circulation. J. Phys. Oceanogr., *13,* 2020–2037.

Rhines, P. B. and W. R. Young. 1982a. A theory of wind-driven circulation I. Mid-ocean gyres. J. Mar. Res., *40* (Suppl.), 559–596.

—— 1982b. Homogenization of potential vorticity in planetary gyres. J. Fluid Mech., *122,* 347–367.

Young, W. R. and P. B. Rhines. 1982. A theory of the wind-driven circulation II. Gyres with western boundary layers. J. Mar. Res., *40,* 849–872.

Received: *2 December, 1985*; revised: *12 May, 1986.*